Impact of graphene encapsulation on thermodynamics of quantum emitters in hexagonal boron nitride

M. K. Prasad
School of Mathematics, Statistics and Physics, Newcastle University, Newcastle upon Tyne NE1 7RU, United Kingdom and Joint Quantum Centre (JQC) Durham-Newcastle, United Kingdom

J. P. Goss*
School of Mathematics, Statistics and Physics, Newcastle University, Newcastle upon Tyne NE1 7RU, United Kingdom

J. D. Mar†
School of Mathematics, Statistics and Physics, Newcastle University, Newcastle upon Tyne NE1 7RU, United Kingdom; Joint Quantum Centre (JQC) Durham-Newcastle, United Kingdom; and Department of Electrical, Computer, and Biomedical Engineering, Toronto Metropolitan University, Toronto, Ontario M5B 2K3, Canada

(Received 14 March 2025; revised 26 June 2025; accepted 30 July 2025; published 2 September 2025)

Color centers in hexagonal boron nitride (hBN) have gained significant interest as single-photon emitters and spin qubits for applications in a wide range of quantum technologies. As the integration of these solid-state quantum emitters into electronic devices necessitates electrical control, it is essential to gain a deeper understanding of the mechanisms for charge control of these defect color centers in hBN/graphene heterostructures. In this article, we show that screening due to the encapsulation of hBN by graphene modifies the electrical levels of hBN, leading to charge transfer. Furthermore, we show that the charged defects have low-energy barriers for defect reorientation which can be overcome by moderate gate voltages. This study shows that accurate modeling of the charge state of the defect is necessary to be able to electrically control defects.

DOI: 10.1103/k155-1t97

I. INTRODUCTION

Defects in hBN have gained significant interest for their applications in quantum technologies, defect-based LEDs and spin-valve devices [1–4]. The architecture of such devices involves hBN being encapsulated within a heterostructure, such as by graphene [5]. It was found that when graphene is interfaced with hBN, emitters were quenched due to charge and energy transfer [6,7], hence it is clear that graphene has a potentially critical role in the control of defects in hBN via electric fields or charge injection [2,6–8]. It is therefore necessary to study the impact of graphene layers on the electrical levels of defects in hBN, noting the modification of electrical levels also has an impact on the response of defects to external electric fields [5,9]. For example, Stark effect experiments show that defects which possess an electric dipole perpendicular to the hBN plane show an inversion of dipole orientations or charging in the presence of strong electric fields parallel to the dipole orientation [5].

Studies have shown that encapsulation with additional hBN layers or different substrate impacts the position of the donor levels with respect to vacuum [10,11]. However, few studies have explored the influence of the environment on the ground-state geometry and spin configurations of defects. It is critical that such information is known when validating experimental results, such as photoluminescence spectra, with theoretical predictions.

In our previous work it was shown that the location of the donor and acceptor levels of defects in hBN relative to the work function of graphene is a valuable predictor for charge transfer between hBN and graphene, and we demonstrated a method using the electronic density of states (DOS) to predict the degree of charge transfer [12]. However, as the electrical levels of defects are sensitive to both strain and external environment, it is of interest to explore if the graphene layers directly impact the electrical levels of defects in hBN [13–15].

In this Letter, using the carbon–nitrogen-vacancy complex (C_BV_N) as an illustrative example, we show that charge transfer occurs when hBN is encapsulated by graphene, although such a process is not considered to be energetically favorable based on calculations of the donor level in isolated monolayer hBN. We also show that due to strain there is a significant out-of-plane distortion of the defect in the charged state and demonstrate that the barrier to the inversion of the direction of the dipole moment is significantly lowered due to charging. This highlights the necessity of accounting for the environment when determining the ground-state configuration

*Contact author: jonathan.goss@ncl.ac.uk
†Contact author: jdmar@torontomu.ca

Published by the American Physical Society under the terms of the Creative Commons Attribution 4.0 International license. Further distribution of this work must maintain attribution to the author(s) and the published article's title, journal citation, and DOI.

of the defect. Our findings therefore contribute significantly to the understanding of electric field control via the Stark effect, electroluminescence, and strain control of hBN quantum emitters.

II. METHODOLOGY

Our DFT calculations were performed using the *Ab Initio* Modeling PROgram [16] (AIMPRO) with periodic boundary conditions and the PBE-GGA exchange-correlation functional [17]. The atoms are modeled using norm-conserving separable pseudopotentials [18]. Kohn-Sham eigenfunctions are represented with a basis of sets of independent *s*- and *p*-Gaussian orbitals [19], with the addition of one (two) sets of *d*-Gaussian functions for C (B and N) atoms to account for polarization. This amounts to 18 independent Gaussian functions per C atom in the basis, and 28 per B and N atom. Additional sets of functions are located in the vacuum regions to ensure accurate representation of the evanescence. The charge density is Fourier transformed using plane waves with an energy cutoff of 300 Ha, leading to energies converged to better than 1 meV with respect to this parameter. The Brillouin zone of the primitive structures were sampled using a $16 \times 16 \times 1$ Monkhorst-Pack scheme [20]; nonprimitive cells employed sampling with the same or denser reciprocal space density. Structures were optimized by the conjugate-gradient method until the total energy changed by less than 10^{-5} Ha, and forces are less than 10^{-4} a.u. The treatment of basis sets, sampling and vacuum lead to the calculation of the optimized in-plane lattice constant of monolayer hBN as 2.514 Å, in good agreement with previous comparable calculations and with the experimental value of 2.504 Å [21–24]. Similarly, our calculated value of 2.47 Å for the lattice constant of monolayer graphene is in excellent agreement with the literature [25].

Band structures shown in this paper have been calculated using $6 \times 6 \times 1$ cells, as dispersion was negligible in this cell size. Where required, calculations using larger cell sizes were also performed to confirm the convergence of properties with cell size.

The vacuum thickness was greater than four interlayer spacings of bulk hBN (Ref. [25]) and van der Waals interactions were represented using the Grimme-D3 scheme [26]. The formation energy of a defect, X, in charge state q is

$$E_f(X,q) = E_{\text{tot}}(X,q) - E_{\text{host}} - \sum_i n_i\mu_i + q(\varepsilon_{\text{VBM}} + \varepsilon_F), \tag{1}$$

where $E_{\text{tot}}(X,q)$ is the total energy of the defective system, E_{host} is the total energy of pristine monolayer hBN of the same size, n_i is the change in the number of atoms of species i relative to pure hBN and μ_i is the chemical potential of the species i. The formation energies were calculated for N-rich conditions specified by $\mu_{\text{N}} + \mu_{\text{B}} = \mu_{\text{hBN}}$, where μ_{N} is half the total energy of an N_2 molecule and μ_{hBN} is the energy per formula unit of monolayer hBN. ε_F is the electron chemical potential relative to the host valence-band maximum (VBM), ε_{VBM}. We have adopted the standard (q/q') notation to denote the charge transition level (CTL) between charges q and q' relative to the VBM. Where the vacuum electrostatic potential has been used as a reference, the potential has been determined from the average in the plane at the halfway point in the vacuum between images.

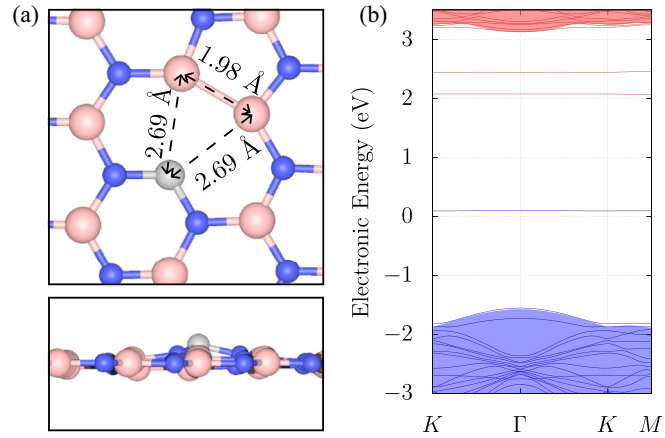


FIG. 1. (a) Schematic of C_BV_N in its singlet ground-state, with pink, blue and gray spheres representing B, N and C, respectively. (b) Shows the corresponding band structure, where the shading indicates the filling of the corresponding defect-free hBN. Blue and red shading indicate occupied and empty bands, respectively. The zero in the energy scale is set to the Dirac point of the pristine graphene.

To mitigate against systematic errors due to periodic boundary conditions (PBCs) in charged systems, we have adopted the uniform scaling of the cell sizes [27,28], leading to an uncertainty of the order of ±0.1 eV in the formation energy [28]. As we consider defects with low charged states, the maximum charge being $|2e|$, we find that the uncertainty in the valence-band position due to the artificial electrostatic field from the charged defect is negligible.

Quantification of charge transfer has been approached by integrating the DOS of the heterostructure from the Fermi level to the small band gap induced by the formation of the heterostructure [12]. Calculations were performed with the net spin either constrained (fixed spin) or allowed to vary during the self-consistency process (free spin). For free spin calculations, the population of the spin channels was based upon Fermi-Dirac statistics with spin-up and spin-down channels having the same self-consistent electron chemical potential.

Nudged elastic band (NEB) calculations were performed using the climbing-image method [29] for a 6×6 supercell and $8 \times 8 \times 1$ k-point sampling to ensure convergence of the Fermi level, and eleven images between the initial and final states was found to sufficiently resolve the energy surface.

III. RESULTS

C_BV_N is formed when carbon substitutes for boron adjacent to a nitrogen vacancy. Interest in C_BV_N has focused on its potential as a source of visible single-photon emission [30,31], particularly as it is among a class of defects with an out-of-plane intrinsic electric dipole, rendering it accessible to Stark tuning via external electric fields [9,32]. The ground-state structure of the defect is a spin singlet, with C_s point-group symmetry due to the out-of-plane movement of the carbon atom [33] [Fig. 1(a)]. The introduction of this

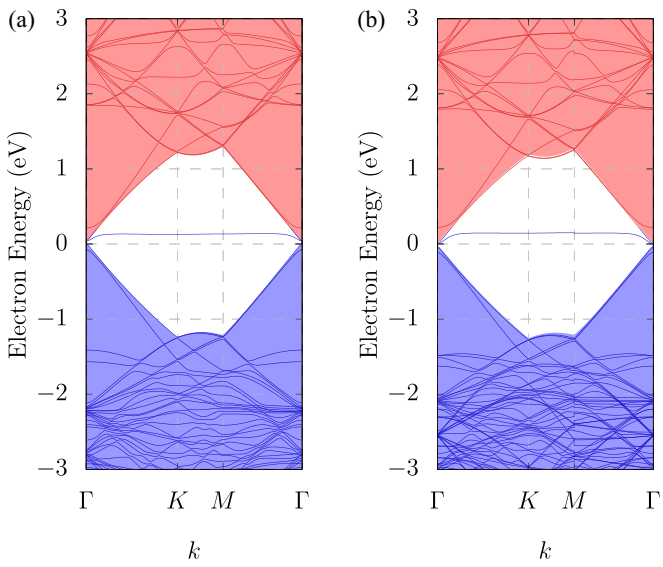


FIG. 2. Band structures of C_BV_N in (a) hBN/Gr and (b) 2-hBN/Gr, with C_BV_N in the hBN layer adjacent to graphene. The zero in the energy scale is set to Dirac point the corresponding the pristine heterostructure. Colors follow Fig. 1.

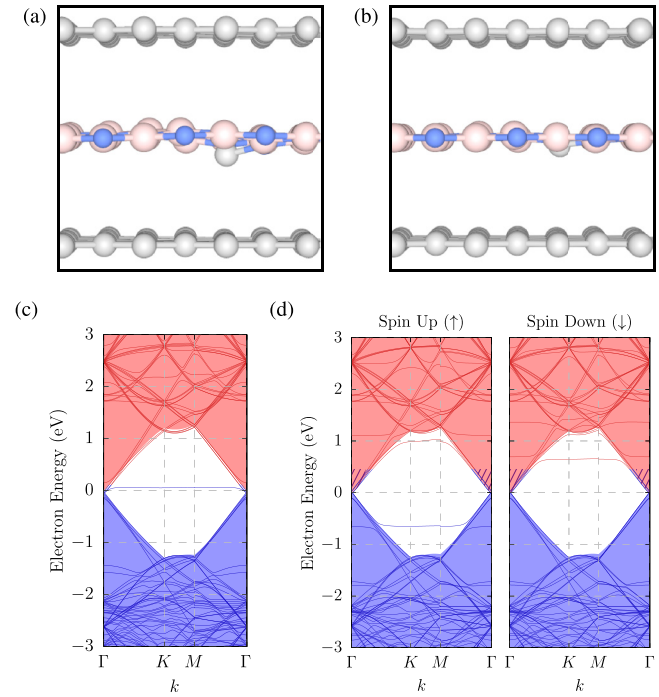


FIG. 3. The side view of C_BV_N in Gr/hBN/Gr in showing the displacement of the carbon atom from the hBN plane in (a) the spin singlet state and (b) the spin doublet state (from free spin calculations). (c) and (d) show the corresponding band structures of the singlet and doublet configurations, respectively. The zero in the energy scale is set to the Dirac point of pristine Gr/hBN/Gr. The hatched shading reflects the occupation of the graphene states due to charge transfer from hBN. Colors follow Fig. 1.

defect leads to one (two) occupied (unoccupied) nondegenerate defect-levels in the band gap [Fig. 1(b)].

The defect when either positively and negatively charged forms a spin doublet, with C_s symmetry geometries [31]. Taking the average z displacement of the boron and nitrogen atoms in the hBN layer, where z is the direction perpendicular to pristine hBN, as the location of the plane, a small, 0.18 Å, out-of-plane distortion in the positively charged defect lowers the energy by ≈2 meV. This has not been captured by previous studies in literature [34]. Although it is a small difference, strain effects significantly enhance the stability of the distorted arrangement, as will be discussed later. The donor and acceptor levels of C_BV_N were calculated at 5.1 and 1.3 eV below vacuum. The work function of graphene was calculated using the same computational framework in our previous work to be 4.3 eV [12], which is consistent with existing calculations of the work function of graphene [35]. Since the donor (acceptor) level lies below (above) the graphene work function, charge transfer is not expected. Free spin structural relaxation of C_BV_N in hBN/Gr resulted in zero effective spin in the system, consistent with the defect remaining in the neutral charge state as determined by explicit calculations of the degree of charge transfer.

A similar result was observed when an additional hBN layer was added to the system, resulting in bilayer hBN on graphene (2-hBN/Gr). No charge transfer was found and the spin-singlet state remained the ground state regardless of the layer location of the defect. This is reflected in the band structures of C_BV_N in both hBN/Gr and 2-hBN/Gr, Fig. 2.

The impact of an additional layer of Gr on hBN/Gr to form Gr/hBN/Gr is now reviewed. Structural relaxation of the defect-free three-layer structure yields an in-plane lattice constant of 2.48 Å, representing 0.5% and −1.4% strains in the graphene and hBN layers relative to the isolated monolayers.

Structural relaxation performed with free spin and fixed spin ($S = 0$) calculations resulted in the carbon atom moving out-of-plane. The carbon atom moved 0.24 nm during free spin relaxation from the hBN plane, significantly less than the 0.54 nm displacement obtained for in the fixed spin-singlet relaxation [Figs. 3(a) and 3(b)]. This contrasts the observation in hBN/Gr and 2-hBN/Gr where the free spin and fixed spin calculations resulted in the same structure. The reason for the difference in the structure can be understood from the magnetic moment in the free-spin case, which is ≈1 μ_B, μ_B being the Bohr magneton. The calculation of charge transfer revealed that ≈e transfers from C_BV_N to graphene, resulting in a spin doublet. This is reflected in the band structures of C_BV_N in Gr/hBN/Gr. The fixed spin $S = 0$ calculation results in the occupied defect level being at the Dirac point, Fig. 3(c), and this does not favor charge transfer. In the free-spin case, Fig. 3(d), the highest occupied defect level shifts higher in energy, above the Dirac point, resulting in charge transfer and a doublet state.

In our calculations, the self-consistently obtained spin doublet corresponding to the transfer of an electron to graphene, is only marginally stable, being just 20 meV lower than the energy obtained for the fixed spin, representing an overall spin-singlet. The calculations were repeated in 8×8 and 10×10 supercells, and the spin doublet is lower in energy (by 99 and 120 meV, respectively). We also established that the vacuum spacing does not impact the energy ordering of

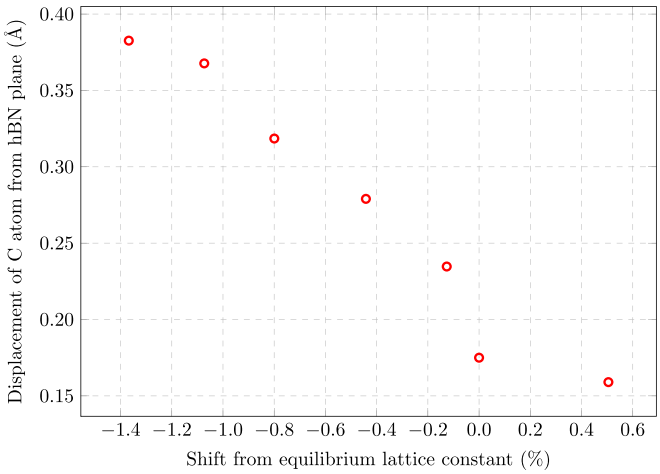


FIG. 4. Displacement of C from the hBN layer in positively charged C_BV_N in monolayer hBN as a function of isotropic biaxial strain.

the $S = 0$ and $S = \frac{1}{2}$ states, reflecting the absence of net polarization between the layers, as determined from the absence of any significant canceling electric field in the vacuum. As charge transfer occurred for Gr/hBN/Gr and not hBN/Gr, we suggest that the electrical levels of C_BV_N are modified when encapsulated by graphene.

There are two significant features of interest in this Gr/hBN/Gr system. First, it was observed that charge transfer occurs only when hBN is encapsulated in graphene. Second, although the geometry of C_BV_N in the positive charged state in isolated hBN is nearly planar in geometry, a significant out-of-plane distortion occurs in the heterostructure.

To explore the latter of these, the positively charged C_BV_N in isolated monolayer hBN was optimized under different biaxial strains. Figure 4 shows that increasing compressive strain leads to an increase in the displacement of the carbon atom from the hBN plane. At approximately −1.4% strain, at which the lattice constant of hBN is equal to that of the heterostructure, the carbon atom is 0.38 Å from the hBN plane. At the same strain, the restriction of the carbon atom to the hBN plane results in a configuration 50 meV higher in energy, highlighting that stabilization due to distortion, although small in unstrained hBN, has physical significance. To determine if strain stabilized the charged defect sufficiently to allow charge transfer to occur in Gr/hBN/Gr, the free-spin and fixed spin calculation with $S = 0$ was repeated with the lattice constant set to that of unstrained hBN. This still resulted in charge transfer, with the free-spin calculation resulting in a magnetic moment of 1 μ_B and the spin-singlet being nearly 200 meV higher in energy. The displacement of the carbon atom in $S = \frac{1}{2}$ was approximately 0.14 Å, which is comparable to the displacement of 0.18 Å of the +1 charged C_BV_N in isolated monolayer hBN. Additionally, the work function of graphene under tensile strain to match the lattice constant of hBN was calculated to be 4.5 eV, which is still above the donor level of C_BV_N, and so strain induced modification of the work function can be eliminated as the source of charge transfer. Therefore, we deduce that strain is not the cause of charge transfer being allowed in Gr/hBN/Gr.

To determine if there was significant hybridization when compared with the positively charged defect in isolated monolayer hBN, Mulliken analysis was performed on the band structure of the defect in Gr/hBN/Gr and compared with the band structure of the defect in monolayer hBN. This is shown in Fig. 5(a). The yellow and black bands reflect a higher localization of the electronic energy levels in hBN and graphene, respectively. Comparing Fig. 5(b) with the yellow bands in Fig. 5(a), it is seen that the band structure of C_BV_N in Gr/hBN/Gr resembles that of the positively charged C_BV_N in isolated monolayer hBN superimposed on the graphene band structure. The location of the defect levels from the valence band edge of hBN, according to the Mulliken analysis, in Gr/hBN/Gr is comparable to that in monolayer hBN. As such, it is unlikely that hybridization is the principal cause of the modification of the electrical levels as this would have resulted in significant differences in the band structure and we can rule out a direct interaction between graphene and hBN being the cause.

As both the spin-singlet and doublet configurations were found in the Gr/hBN/Gr heterostructure, we sought to understand the barrier to move between the two states (noting that displacement of C above and below the hBN plane are equivalent by symmetry). The barrier between the two directions of displacement was investigated for $S = 0$ and $S = \frac{1}{2}$ states, the result of these NEB calculations being presented in Fig. 6.

The NEB data for the 6×6 supercell show the charge-transfer, nonzero effective spin case (circles and triangles in Fig. 6), is energetically favored throughout the inversion process. The energy difference between the minimum in the $S = 0$ state (black squares) and the free-spin case (red circles) converges to around 120 meV for large cells. Although there appears to be a minimum at 0.45 Å (blue triangles), it represents a state with partial charge transfer and disappears in larger cells. Free-spin structural optimization starting with the relaxed structure of the $S = 0$ state in a larger cell ($8 \times 8 \times 1$), converged to the structure and magnetic moment of the $S = \frac{1}{2}$ state. As it did not result in an intermediate state with partial charge transfer, it is not considered to be a metastable state. The increase in the energy difference is attributed to the convergence of the effective spin from 0.98 μ_B to 1 μ_B with cell-size for the 8×8 and 10×10 cells, consistent with the convergence of the degree of charge transfer. For the data shown by circles the effective spin remain close to $\frac{1}{2}$, indicating that charge-transfer is constant through this range, and the out-of-plane displacement stabilizes the defect. The barrier to move between the two orientations where charge-transfer occurs is 30 meV, whereas for the fixed spin-singlet case the barrier is 280 meV.

For comparison with a system where no charge transfer is observed, the energy profile (Fig. 7) for flipping the carbon orientations for the spin singlet and doublet states are shown for C_BV_N in 2-hBN/Gr, where the calculations were performed with fixed spin. At the minima in the $S = \frac{1}{2}$ curve, the singlet configuration is lower in energy for the same displacement of the carbon atom. Hence, a repetition of the structural relaxation with free spin converges to the $S = 0$ equilibrium configuration. Comparing Gr/hBN/Gr with 2-hBN/Gr (Figs. 6 and 7), suggests that the donor level has risen above the Dirac point due to the inclusion of the second

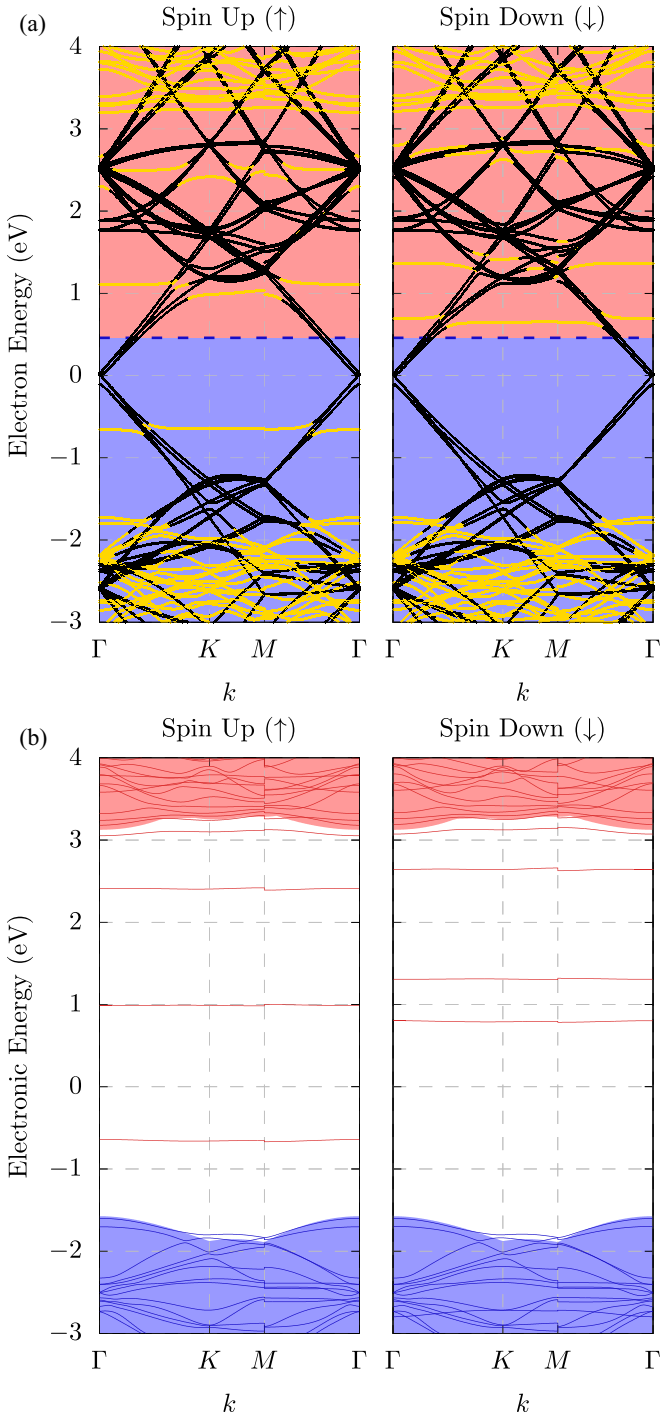


FIG. 5. (a) Band structure of C_BV_N in Gr/hBN/Gr where the localization of the bands as determined by Mulliken analysis is indicated by color. The black (yellow) lines correspond to electronic levels with higher degree of localization in the graphene (hBN) layers. Background colors separate occupied (blue) and unoccupied (red) regions based on the Fermi level. (b) Band structure of $C_BV_N^+$ in isolated monolayer hBN. Color schemes follow Fig. 1. The zero on the energy scale has been set to the Dirac point in pristine Gr/hBN/Gr for panel (a) and pristine Gr in panel (b).

graphene layer, leading to charge transfer. The band structures also support this conclusion. Comparing Figs. 2(a), 2(b) and 3(c), the location of the occupied defect level with respect to

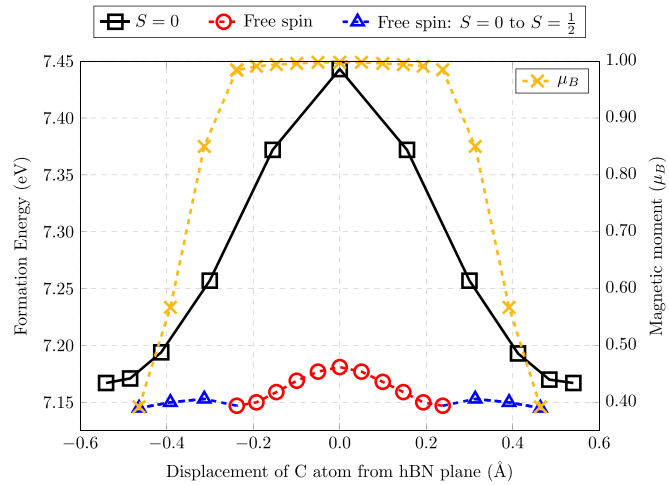


FIG. 6. Energies for the NEB path between the equilibrium configurations of the spin singlet state (squares), doublet state (circles), and between the singlet and doublet states (triangles). Crosses show the variation in μ_B for the free spin case.

the Dirac point is very similar, and lack of charge transfer is observed in each of these cases. However, in Fig. 3(d) the occupied state is above the Dirac point and indicates a shift in the donor level.

IV. DISCUSSION

We now comment on the implications for the observable optical properties based upon our findings. It is clear from Figs. 6 and 7 that the encapsulating environment has a significant effect on the C_BV_N charge transition levels. Similar phenomena were previously predicted in a study on the variation of the charge transition levels (CTLs) of hBN with encapsulating hBN layers, SiO_2 and diamond substrates [10,11]. Here we find that additional Gr layers have a much greater effect on the CTLs than hBN layers. From the Mulliken analysis, no significant differences were

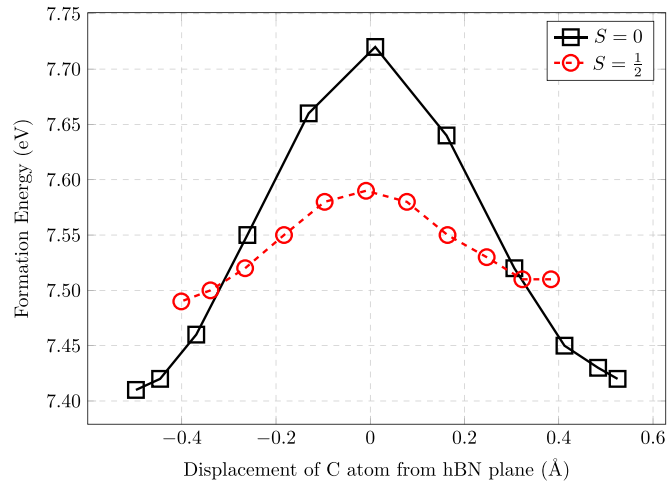


FIG. 7. The variation of the formation energy of C_BV_N along the energy path for $S = 0$ (squares) and $S = \frac{1}{2}$ (circles) configurations in 2-hBN/Gr.

observed when comparing the spin-doublet C_BV_N configuration in Gr/hBN/Gr with the band structure of $C_BV_N^+$ in isolated monolayer hBN. Hence, the bonding nature of the defect is unchanged and the principal reason for the shift in ionization energies comes from electrostatic effects. The change may be attributed to the large difference in the electric permittivities of hBN and graphene. The metallic nature of the graphene layers lead to a greater screening of the localized charge in the defect than hBN or vacuum. This subsequently lowers the ionization energy of the defect and shifts the donor level above the Dirac point of graphene. To achieve a similar effect using hBN would require a larger thickness of hBN. As such, unlike in 2-hBN/Gr and 1-hBN/Gr systems, charge-transfer is predicted for Gr/hBN/Gr. This will be especially relevant in systems where multilayer hBN is sandwiched between graphene gates for the application of electric fields and charge injection [5,8,9,36].

In monolayer hBN there is a small displacement of the carbon atom from the hBN plane for $(C_BV_N)^+$, and the effect is enhanced in the heterostructures. As illustrated by the data in Fig. 4, displacement of carbon from the hBN plane is stabilized by increasing compressive biaxial strain. However, the stabilization of the distorted arrangement of the charged defect due to strain was not determined to be the cause of charge transfer in Gr/hBN/Gr, as charge transfer occurred in the system even when the hBN layer was unstrained. Therefore, under strain or via the influence of the substrate, even the positively charged defect can be tuned by an electric field perpendicular to the hBN plane because it possesses a component of the electric dipole moment parallel to the applied field. However, the low barrier between the two minima of $(C_BV_N)^+$ suggests that low gate voltages are sufficient for the atoms to overcome the barrier and flip to the site on the opposite side of the plane. This would invert the orientation of the dipole with respect to the field and subsequently, the direction of the Stark shift. Studies on Stark tuning of hBN emitters have found V-shaped variations of zero-phonon line with applied field, which supports the occurrence of such processes [5]. It is also possible that some defects can possess charged configurations within the barrier of transition and act as metastable intermediate states for the transition between sites.

Furthermore, we can understand the increase in the rate of flipping between the two sites due to charge transfer from transition state theory (TST) [37]. According to TST, the rate can be calculated as

$$k_{A\to B} = \nu \exp\left(-\frac{E_B}{k_B T}\right), \tag{2}$$

where $k_{A\to B}$ is the rate at which the transition occurs between the two equilibrium sites, ν is the attempt frequency which is usually in the order of 10^{12}–10^{13} Hz [37], E_B is the barrier to the transition, k_B is the Boltzmann constant, and T is the temperature ($k_BT = 25$ meV at room temperature). As E_B for the spin-singlet and doublet states are 280 meV and 30 meV respectively, the flipping rates for the singlet and doublet states are calculated to be 1.4×10^8 and 3.0×10^{12} Hz, respectively. Hence, charge transfer due to graphene encapsulation exponentially enhances the transition rate by 10^4, independent of the attempt frequency. Therefore, significant differences in the spectroscopic properties can be observed for the same defect in isolated hBN and Gr/hBN/Gr.

When the NEB calculation for flipping was performed for neutral C_BV_N in isolated monolayer hBN, the barrier to transition was found to be 480 meV, leading to a rate of 4.6×10^4 Hz. Spectroscopically, the charged defect in Gr/hBN/Gr would experience an averaged potential due to the transition rate being much higher than the radiative recombination rate (which is on the order of 10^9 Hz in hBN [1]), and inhomogeneous broadening would be suppressed, whereas in monolayer hBN, the neutral defect can exhibit spectral jumps on millisecond timescales and significant inhomogeneous broadening. Therefore, the surrounding material can impact properties such as coherence times, which are of significance for the exploitation of these defects as qubits or single-photon sources. Hence, the same defect in Gr/hBN/Gr would exhibit different PL spectra when compared with the single-sided hBN/Gr case, as the former would correspond to the charged defect and the latter to the neutral case. Furthermore, there would be differences in the zero-phonon line (ZPL) lineshape of the defect in Gr/hBN/Gr and single-sided cases due to the variation in the homogeneity of the broadening mechanisms.

We also estimated the tunneling rate for the carbon atom for $S = \frac{1}{2}$ in Gr/hBN/Gr using the WKB scheme. This is given by

$$t_{A\to B} = \nu \exp\left(-\frac{2}{\hbar}\int \sqrt{2m_C\phi(x)}dx\right), \tag{3}$$

where $t_{A\to B}$ is the tunneling rate, $\phi(x)$ is the barrier energies given by the images in free spin path (red circles) in the NEB calculation in Fig. 6 with the energy at the minima taken to be zero and m_C is the mass of the carbon atom. The exponential product in Eq. (3) gives the tunneling probability and the factor of ν, which was taken to be the same attempt frequency as the thermal process, converts the probability to a tunneling rate. This results in a tunneling probability of e^{-16} and a tunneling rate of 1.1×10^6 Hz. As the rate for the thermal process for flipping is approximately 10^6 times greater than the tunneling rate, the contribution of tunneling to the flipping of the orientation of the carbon atom can be ignored. Furthermore, the barrier heights and widths for the $S = 0$ state in Gr/hBN/Gr and all spin-states in the single-sided systems are wider and higher and the corresponding tunneling probabilities are expected to be even lower in these systems and can also be neglected.

As the energy difference between the spin singlet and doublet configurations is ≈120 meV, continued increase in the applied voltages, which is taken as the difference in the Fermi levels of the top and bottom Gr layers, would likely lead to a change in the charge state and turn the emitter dark or change its emission wavelength. This is because the potential well of the singlet state could be lowered to below the charged doublet state, and the defect transitions from the doublet to the singlet state. Graphene has been known to quench emission from hBN when used as a substrate as it can cause a change in the charge state of the defect [6]. Even if the defect remains optically active after charge transfer, the change in the orientation of the electric dipole moment would manifest as an abrupt change in the polarization and degree

of Stark shift. The lowering of the barrier to transition due to an applied field can dramatically increase the tunneling probability, due to the exponential dependence of the tunneling probability on the barrier height, Eq. (3). The tunneling rate calculated for C_BV_N in $S = \frac{1}{2}$ in Gr/hBN/Gr also assumed that the transition occurred from the minimum in energy of the energy profile. Thermal energy, due to the experiment being performed at higher temperatures, can excite the defect to higher vibrational states and the barrier height experienced by the defect is then lowered, which can then increase tunneling and thermal flipping rates.

V. CONCLUSION

In this work, we have shown that the encapsulation of hBN by graphene layers leads to dramatic modifications in the electrical levels. Using C_BV_N as an illustrative example, we show that the donor level shifts toward the conduction band due to additional graphene layers, leading to charge transfer. The effect is principally due to the different screening when the defect is encapsulated entirely in graphene, when compared with graphene and hBN. NEB modeling also shows that the barrier to the flipping of the carbon atom across the hBN plane is relatively low and would likely to lead to a V-shaped Stark shift, such as illustrated in Ref. [5]. We have also estimated the flipping rates using TST and WKB tunneling rates and showed that the dominant process is thermal. It is therefore imperative that in determining viable color centers for single-photon emitters that may be controlled by an external electric field, the correct charge state, strain and substrate are explicitly modeled. Also, the complex interplay between the dielectric environment and strain led to defect geometries that can differ significantly from the monolayer case and has implications on spectroscopic properties, such as the response to external electric fields and the degree of phonon coupling. The results of this work will therefore have a significant impact on the electric field, charge and strain control of quantum emitters in hBN for applications in quantum technologies.

DATA AVAILABILITY

The data that support the findings of this article are openly available [38].

[1] T. T. Tran, K. Bray, M. J. Ford, M. Toth, and I. Aharonovich, Quantum emission from hexagonal boron nitride monolayers, Nat. Nanotechnol. **11**, 37 (2016).

[2] M. Grzeszczyk, K. Vaklinova, K. Watanabe, T. Taniguchi, K. S. Novoselov, and M. Koperski, Electroluminescence from pure resonant states in hBN-based vertical tunneling junctions, Light: Sci. Appl. **13**, 155 (2024).

[3] P. U. Asshoff, J. L. Sambricio, S. Slizovskiy, A. P. Rooney, T. Taniguchi, K. Watanabe, S. J. Haigh, V. Fal'ko, I. V. Grigorieva, and I. J. Vera-Marun, Magnetoresistance in Co-hBN-NiFe tunnel junctions enhanced by resonant tunneling through single defects in ultrathin hBN barriers, Nano Lett. **18**, 6954 (2018).

[4] M. K. Prasad, M. P. Taverne, C.-C. Huang, J. D. Mar, and Y.-L. D. Ho, Hexagonal boron nitride based photonic quantum technologies, Materials **17**, 4122 (2024).

[5] G. Noh, D. Choi, J. H. Kim, D. G. Im, Y. H. Kim, H. Seo, and J. Lee, Stark tuning of single-photon emitters in hexagonal boron nitride, Nano Lett. **18**, 4710 (2018).

[6] Z. Q. Xu, N. Mendelson, J. A. Scott, C. Li, I. H. Abidi, H. Liu, Z. Luo, I. Aharonovich, and M. Toth, Charge and energy transfer of quantum emitters in 2D heterostructures, 2D Mater. **7**, 031001 (2020).

[7] J. C. Stewart, Y. Fan, J. S. Danial, A. Goetz, A. S. Prasad, O. J. Burton, J. A. Alexander-Webber, S. F. Lee, S. M. Skoff, V. Babenko, and S. Hofmann, Quantum emitter localization in layer-engineered hexagonal boron nitride, ACS Nano **15**, 13591 (2021).

[8] M. Yu, D. Yim, H. Seo, and J. Lee, Electrical charge control of h-BN single photon sources, 2D Mater. **9**, 035020 (2022).

[9] A. Scavuzzo, S. Mangel, J. H. Park, S. Lee, D. L. Duong, C. Strelow, A. Mews, M. Burghard, and K. Kern, Electrically tunable quantum emitters in an ultrathin graphene-hexagonal boron nitride van der Waals heterostructure, Appl. Phys. Lett. **114**, 062104 (2019).

[10] D. Wang and R. Sundararaman, Substrate effects on charged defects in two-dimensional materials, Phys. Rev. Mater. **3**, 083803 (2019).

[11] D. Wang and R. Sundararaman, Layer dependence of defect charge transition levels in two-dimensional materials, Phys. Rev. B **101**, 054103 (2020).

[12] M. K. Prasad, O. A. Al-Ani, J. P. Goss, and J. D. Mar, Charge transfer due to defects in hexagonal boron nitride/graphene heterostructures: An *ab initio* study, Phys. Rev. Mater. **7**, 094003 (2023).

[13] M. G. Sensoy, D. Vinichenko, W. Chen, C. M. Friend, and E. Kaxiras, Strain effects on the behavior of isolated and paired sulfur vacancy defects in monolayer MoS_2, Phys. Rev. B **95**, 014106 (2017).

[14] U. Aschauer and N. A. Spaldin, Interplay between strain, defect charge state, and functionality in complex oxides, Appl. Phys. Lett. **109**, 031901 (2016).

[15] C. Deger, S. Tan, K. Houk, Y. Yang, and I. Yavuz, Lattice strain suppresses point defect formation in halide perovskites, Nano Res. **15**, 5746 (2022).

[16] R. Jones and P. Briddon, "Chapter 6 the *ab initio* cluster method and the dynamics of defects in semiconductors," in *Identification of Defects in Semiconductors*, Semiconductors and Semimetals, edited by M. Stavola (Elsevier, 1998), Vol. 51, pp. 287–349.

[17] J. P. Perdew, K. Burke, and M. Ernzerhof, Generalized gradient approximation made simple, Phys. Rev. Lett. **77**, 3865 (1996).

[18] C. Hartwigsen, S. Goedecker, and J. Hutter, Relativistic separable dual-space Gaussian pseudopotentials from H to Rn, Phys. Rev. B **58**, 3641 (1998).

[19] J. P. Goss, M. J. Shaw, and P. R. Briddon, Marker-method calculations for electrical levels using Gaussian-orbital basis

sets, in *Theory of Defects in Semiconductors*, Topics in Applied Physics, edited by D. A. Drabold and S. K. Estreicher (Springer, Berlin/Heidelberg, 2007), Vol. 104, pp. 69–94.

[20] H. J. Monkhorst and J. D. Pack, Special points for Brillouin-zone integrations, Phys. Rev. B **13**, 5188 (1976).

[21] L. Cai, X. Fan, H. Su, M. Lv, and B. Xu, First principles calculation of the lattice constants of hexagonal and cubic boron nitride to 3000 K and 30 Gpa, Ferroelectrics **566**, 136 (2020).

[22] B. Xu, M. Lv, X. Fan, W. Zhang, Y. Xu, and T. Zhai, Lattice parameters of hexagonal and cubic boron nitrides at high temperature and high pressure, Integr. Ferroelectr. **162**, 85 (2015).

[23] A. Janotti, S.-H. Wei, and D. J. Singh, First-principles study of the stability of BN and C, Phys. Rev. B **64**, 174107 (2001).

[24] M. Topsakal, E. Aktürk, and S. Ciraci, First-principles study of two- and one-dimensional honeycomb structures of boron nitride, Phys. Rev. B **79**, 115442 (2009).

[25] J. Wang, F. Ma, and M. Sun, Graphene, hexagonal boron nitride, and their heterostructures: Properties and applications, RSC Advances **7**, 16801 (2017).

[26] S. Grimme, Density functional theory with London dispersion corrections, Wiley Interdiscip. Rev. Comput. Mol. Sci. **1**, 211 (2011).

[27] H.-P. Komsa, N. Berseneva, A. V. Krasheninnikov, and R. M. Nieminen, Charged point defects in the flatland: Accurate formation energy calculations in two-dimensional materials, Phys. Rev. X **4**, 031044 (2014).

[28] H.-P. Komsa, N. Berseneva, A. V. Krasheninnikov, and R. M. Nieminen, Erratum: Charged point defects in the flatland: Accurate formation energy calculations in two-dimensional materials [Phys. Rev. X **4**, 031044 (2014)], Phys. Rev. X **8**, 039902(E) (2018).

[29] G. Henkelman, B. P. Uberuaga, and H. Jónsson, A climbing image nudged elastic band method for finding saddle points and minimum energy paths, J. Chem. Phys. **113**, 9901 (2000).

[30] A. Sajid and K. S. Thygesen, V_NC_B defect as source of single photon emission from hexagonal boron nitride, 2D Mater. **7**, 031007 (2020).

[31] N. Mendelson, D. Chugh, J. R. Reimers, T. S. Cheng, A. Gottscholl, H. Long, C. J. Mellor, A. Zettl, V. Dyakonov, P. H. Beton, S. V. Novikov, C. Jagadish, H. H. Tan, M. J. Ford, M. Toth, C. Bradac, and I. Aharonovich, Identifying carbon as the source of visible single-photon emission from hexagonal boron nitride, Nat. Mater. **20**, 321 (2021).

[32] S. A. Tawfik, S. Ali, M. Fronzi, M. Kianinia, T. T. Tran, C. Stampfl, I. Aharonovich, M. Toth, and M. J. Ford, First-principles investigation of quantum emission from hBN defects, Nanoscale **9**, 13575 (2017).

[33] C. Linderälv, W. Wieczorek, and P. Erhart, Vibrational signatures for the identification of single-photon emitters in hexagonal boron nitride, Phys. Rev. B **103**, 115421 (2021).

[34] G. Cheng, Y. Zhang, L. Yan, H. Huang, Q. Huang, Y. Song, Y. Chen, and Z. Tang, A paramagnetic neutral C_BV_N center in hexagonal boron nitride monolayer for spin qubit application, Comput. Mater. Sci. **129**, 247 (2017).

[35] D. Ziegler, P. Gava, J. Güttinger, F. Molitor, L. Wirtz, M. Lazzeri, A. M. Saitta, A. Stemmer, F. Mauri, and C. Stampfer, Variations in the work function of doped single-and few-layer graphene assessed by Kelvin probe force microscopy and density functional theory, Phys. Rev. B **83**, 235434 (2011).

[36] S. J. U. White, T. Yang, N. Dontschuk, C. Li, Z.-Q. Xu, M. Kianinia, A. Stacey, M. Toth, and I. Aharonovich, Electrical control of quantum emitters in a Van der Waals heterostructure, Light: Sci. Appl. **11**, 186 (2022).

[37] D. S. Sholl and J. A. Steckel, *Density Functional Theory: A Practical Introduction* (John Wiley & Sons, 2022).

[38] M. K. Prasad, J. P. Goss, and J. D. Mar, Raw data for Figs. 4, 6, and 7 in the journal article: Impact of graphene encapsulation on thermodynamics of quantum emitters in hexagonal boron nitride (2025), 10.25405/data.ncl.29161769.v1.